

Solar internal rotation from LOWL data

A 2D regularized least-squares inversion using B-splines

T. Corbard¹, G. Berthomieu¹, P. Morel¹, J. Provost¹, J. Schou², and S. Tomczyk³

¹ Laboratoire G.-D. Cassini, CNRS URA 1362, Observatoire de la Côte d'Azur, BP 229, F-06304 Nice Cedex 4, France

² Hansen Experimental Physics Laboratory, Annex A201, Stanford University, Stanford, CA 94305-4085, USA

³ High Altitude Observatory, National Center for Atmospheric Research, Boulder, CO 80307, USA

Received 9 December 1996 / Accepted 21 January 1997

Abstract. Observations of surface oscillations of the Sun can be analyzed to probe the solar interior. We use data obtained by the LOWL instrument (LOWL is an abbreviation for low degree with degree denoted by L) installed on Mauna Loa, Hawaii, since 1994 to investigate solar internal rotation. A 2 Dimensional Regularized Least-Squares (2D RLS) inverse method based on an expansion of the solution on B-splines of arbitrary order is presented and applied to a 2 year dataset. This method insures the regularity of the solution in the center and introduces surface constraints. The choice of trade-off parameters in the regularization term is discussed using an L-curves analysis and we discuss the influence of the choice of the order of derivatives in the regularization terms for the description of the deep interior. We study the latitudinal resolution of the inversion of a-coefficients compared to that of the inversion of individual splittings built from these coefficients.

Compared to the previous inversion of the first three months of LOWL data made by Tomczyk et al. (1995b), our solution is extended up to the surface by adding high degree modes and constraining the rotation to fit the spectrographic observations (Snodgrass 1984). In the radiative zone we obtain more rigid rotation and our solution is compatible with a rotation of the solar core of the order or smaller than the surface rotation at mid latitude.

Key words: Sun: interior – Sun: oscillations – Sun: rotation – methods: numerical

1. Introduction

One of the main interests of helioseismology is the description of the Sun's internal rotation rate versus depth and latitude. Over the past decade, increasingly accurate observational data have

become available from ground based observations (e.g. Chaplin et al. 1996; Harvey et al. 1996; Lazrek et al. 1996; Woodard & Libbrecht 1993; Appourchaux et al. 1994; Tomczyk et al. 1995a). These and other datasets have allowed several teams to infer the solar internal rotation profile using 1D (Duvall et al. 1984), 1.5D (Christensen-Dalsgaard & Schou 1988; Dziembowski et al. 1989) and 2D (Sekii 1990, Schou 1991) inversion codes (see Schou et al. (1994) for a more complete list of historical references). All these inversions tend to show a rotation profile which is approximately constant on radii throughout the convection zone, with a sharp transition to a latitudinal independent rotation rate below the base of the convection zone.

One of the objectives of the Global Oscillations at Low Frequency (GOLF, Gabriel et al. 1995), Michelson Doppler Imager (MDI, Scherrer et al. 1995) and Variability of solar IRadiance and Gravity Oscillations (VIRGO, Fröhlich et al. 1995) experiments aboard the SOLar and Heliospheric Observatory (SOHO) satellite is to obtain a more accurate set of measurements of low- and high-degree acoustic modes in order to specify what happens in the deep interior ($r/R_{\odot} < 0.4$), near the surface ($r/R_{\odot} > 0.85$) and in the transition zone below the convection zone. Nevertheless, ground-based experiments have been operating for many years and can provide spectra obtained over much longer time periods than are currently available to the SOHO experiments. In particular, in this paper we use data from the LOWL experiment covering a two year period of observation on which we apply a 2D RLS inversion code using an approximation of the rotation rate by piecewise polynomials projected on a B-splines tensorial product.

We briefly present the well known forward problem in Sect. 2 and discuss the relevant hypothesis and the boundary conditions for the rotation rate. In Sect. 3 we recall basic principles for the 2D RLS method. We present the LOWL data and discuss the choice of inversion parameters for this particular dataset in Sect. 4. The results of inverting the observed frequency splittings are presented in Sect. 5, and our conclusions are presented in Sect. 6. In addition, Appendices A and B give some details about splines basis and the minimization process

and Appendix C recalls the concept of averaging kernels for a linear inversion.

2. Forward problem and hypothesis

2.1. Basic equations

The Sun is oscillating simultaneously in many thousands of global acoustic modes. The observation of these modes at the solar surface and the knowledge of their sub-surface properties are the basis by which helioseismology can sound the interior of the Sun.

Each mode can be described by three integers: the degree l , the azimuthal order m and the radial order n . In a spherically symmetric non-rotating star the eigenfrequencies of the modes are independent of m . The rotation of the Sun induces a preferred axis of symmetry and the frequency difference between westward and eastward propagating waves on the solar surface contains the signature of the global rotation of the Sun.

The rotation period for the Sun (about 1 month) is very long compared to the periods of the observed p-modes (about 5 minutes), thus we can use a linear perturbation theory to predict the effect of rotation on the p-modes. According to this theory and under the assumption that the effect of the magnetic field is negligible, the difference between the frequency ν_{nlm} of a mode with azimuthal order m and the frequency ν_{nl} that this mode would have in a non-rotating (but otherwise identical) star is given in terms of the eigenfunctions of the non rotating star (e.g. Hansen et al. 1977; Christensen-Dalsgaard & Berthomieu 1991).

If we denote by ξ_{nl} and η_{nl} the radial and horizontal displacement of the fluid from its equilibrium position, the displacement ξ has the form:

$$\xi(r, \theta, \phi, t) = \left(\xi_{nl}(r) Y_l^m(\theta, \phi), \eta_{nl}(r) \frac{\partial Y_l^m(\theta, \phi)}{\partial \theta}, \frac{\eta_{nl}(r)}{\sin(\theta)} \frac{\partial Y_l^m(\theta, \phi)}{\partial \phi} \right) e^{2i\pi\nu_{nlm}t}, \quad (1)$$

where (r, θ, ϕ) are the spherical polar coordinates defined from the solar rotation axis $\theta = 0$ and $Y_l^m(\theta, \phi)$'s are spherical harmonics. The so-called frequency splitting $\Delta\nu_{nlm} = \nu_{nlm} - \nu_{nl}$ can be written as a weighted average of the unknown rotation rate Ω :

$$\Delta\nu_{nlm} = m \int_0^{R_\odot} \int_0^1 K_{nlm}(r, \mu) \Omega(r, \mu) dr d\mu \quad (2)$$

with $\mu = \cos(\theta)$ and where the full kernels K_{nlm} derived from the first order perturbation theory are given by:

$$K_{nlm}(r, \mu) = \frac{(2K_{nl}(r)G_{ml}(\mu) + \eta_{nl}^2(r)X_{ml}(\mu))\rho(r)r^2}{I_{nl}}, \quad (3)$$

with:

$$\begin{cases} K_{nl}(r) = \xi_{nl}(r)^2 + (L^2 - 1)\eta_{nl}(r)^2 - 2\xi_{nl}(r)\eta_{nl}(r), \\ G_{ml}(\mu) = P_l^m(\mu)^2, \\ X_{ml}(\mu) = (1 - \mu^2) \frac{d^2}{d\mu^2} (G_{ml}), \\ I_{nl} = \int_0^{R_\odot} [\xi_{nl}(r)^2 + L^2\eta_{nl}(r)^2] \rho(r)r^2 dr, \end{cases} \quad (4)$$

where $P_l^m(\mu)$ are normalized Legendre polynomials, $\rho(r)$ is the density and $L^2 = l(l + 1)$.

In first approximation, we can neglect terms with first and second derivatives of the rotation rate (by partial integration with respect to the colatitude of Eq.(2)) assuming that one has smooth variation in latitude and the so-called rotational kernel reduces to (Cuypers 1980):

$$\tilde{K}_{nlm}(r, \mu) = \frac{K_{nl}(r)G_{ml}(\mu)\rho(r)r^2}{I_{nl}}, \quad (5)$$

The radial part $K_{nl}(r)$ of the rotational kernel is the same as in the 1D inversion problem where the rotation is supposed to be latitudinal independent i.e. $\Omega(r, \mu) = \Omega(r)$ (e.g. Gough 1981). The kernel Eq. (3) is symmetric about the equator and the factor of two is introduced by the assumption that the rotation rate has a similar symmetry property i.e. $\Omega(r, -\mu) = \Omega(r, \mu)$. The functions $\xi_{nl}(r)$, $\eta_{nl}(r)$ are determined by solving the differential equations describing the motion of a self-gravitating fluid body in a standard solar model (Unno et al. 1989).

We note that the approximation Eq. (5) of the rotational kernel includes a term $-\eta_{nl}(r)^2$ which does not appear in Sekii's approximation (Sekii 1993) and which becomes of significant importance compared to the $l(l + 1)\eta_{nl}(r)^2$ term only for the low l . For higher degree modes, this kernel reduces to Sekii's approximation and the terms of Eq. (3) that are neglected have been shown by Pijpers and Thompson (1996) to be small compared to \tilde{K}_{nlm} except near the inner turning point of the modes. Therefore their contribution to the integral Eq. (2) is negligible for the observed modes. Nevertheless, while this approximation of the rotational kernel simplifies the problem and decreases the number of calculations, our work takes into account the full kernel and this should have a significant effect especially if f- or even g-modes become available. We note however that, for the present data, using the full or the approximate kernel leads to the same solution in the zones that are sounded by the observed modes.

The object of all the 2D inversion codes is to infer the rotation rate versus depth and latitude $\Omega(r, \mu)$ from the observed splittings $\Delta\nu_{nlm}$ by inverting the integral relation Eq.(2).

2.2. Boundary conditions

2.2.1. At the surface

Some direct observations of the rotation at the solar surface are available and one may want to force the inferred rotation to match the observed surface rotation. The sidereal rotational frequencies are obtained as a function of latitude at the solar surface by different techniques such as the Doppler shift of photospheric spectral lines or by tracking sunspots, small magnetic features or supergranulation cells (see the review by Schröter (1985)). The values which are derived are within a few percent but they lead to a different variation of the solar rotation as a function of latitude during the solar cycle. These differences could be explained by the different depths where indicators are anchored but a complete interpretation of these observations is strongly

related to a better theoretical understanding of the interaction between rotation, convection and magnetic fields.

The rotation of surface layers has been determined spectroscopically from standard techniques used at Mount Wilson by Snodgrass (1984). In this work we use the rotation results from Doppler velocity measurements made at the Mount Wilson 150 foot tower telescope between 1967 and 1984 and related by Snodgrass & Ulrich (1990). The sidereal plasma rotation rate averaged over the entire period is given by:

$$\Omega_p = A_p + B_p \mu^2 + C_p \mu^4 \begin{cases} A_p = 453.8 \pm 1.0 \text{ nHz} \\ B_p = -54.6 \pm 0.8 \text{ nHz} \\ C_p = -75.4 \pm 1.1 \text{ nHz} \end{cases} \quad (6)$$

All the magnetic tracers are believed to represent the rotation of deeper layers. The observation of small magnetic features leads to a rotation rate slower than the rotation rate of the supergranular pattern but faster than the rotation rate of sunspot groups or the plasma (Komm & Howard 1993). Thus it gives a mean value of the rotation rates estimated by the different indicators and we also use these data to study the sensitivity of the inversion to different surface constraints. The fit of the main sidereal rotational rate of small magnetic features that we use is given by Komm & Howard (1993) from the analysis of magnetograms taken with the NSO Vacuum Telescope on Kitt peak between 1975 and 1991:

$$\Omega_m = A_m + B_m \mu^2 + C_m \mu^4 \begin{cases} A_m = 463.6 \pm 0.7 \text{ nHz} \\ B_m = -64.5 \pm 4.3 \text{ nHz} \\ C_m = -67.2 \pm 4.8 \text{ nHz} \end{cases} \quad (7)$$

The surface rates (Eqs. (6), (7)) are averaged over a long period and are not contemporaneous with the LOWL observations. Moreover they describe the rotation of layers that are not necessarily strictly the solar surface. This might introduce spurious effects in the inversion results if these observations were used as strong constraints. For this reason, we choose to take into account these data in a more flexible way by introducing a parameter λ_s as explained in Appendix B and discussed in Sect. 4.2.3.

2.2.2. At the center

At the limit $r = 0$ the rotation rate Ω has no latitudinal dependence. Thus the functional space where we search the rotation rate must generate only functions which are in agreement with the physical condition:

$$\lim_{r \rightarrow 0} \frac{\partial \Omega(r, \mu)}{\partial \theta} = 0. \quad (8)$$

This condition insures the regularity of the solution at the center and is easy to insert in the inversion process as discussed in Appendix A.

3. The inversion method

The problem of inverting Eq. (2) is intrinsically an ill-posed problem because of its global (or integral) nature (e.g.

Craig & Brown 1986). Furthermore this is strengthened in the helioseismic case because of the lack of modes able to sound the deepest and shallowest layers of the Sun: only a small percentage of the observed p-modes have their corresponding rotational kernels Eq. (3) with significant amplitude below $0.4R_\odot$ or with their lower turning point between $0.95R_\odot$ and the surface (see Fig. 2). Then the solution is not well constrained at these depths and the global nature of the problem implies that this leads to difficulties in the whole domain and that there is no unique solution for the problem.

In order to discretize Eq. (2), we project the unknown rotation rate on a tensorial product of B-splines (see Appendix A):

$$\Omega(r, \mu) = \sum_{p=1}^{n_r} \sum_{q=1}^{n_\mu} \omega_{pq} \varphi_p(r) \psi_q(\mu). \quad (9)$$

Then, we apply a regularized least-squares method on values of both observed splittings and observed surface rotation in order to find the set of coefficients ω_{pq} . The aim of regularization is to stabilize the inversion process by ruling out rapidly oscillating solutions which are physically unacceptable.

In our inversion we adopt a Tikhonov regularization method (Tikhonov & Arsenin 1977) by solving:

$$\min_{\Omega} (J(\Omega) + T(\Omega)), \quad (10)$$

where $J(\Omega)$ is the least-squares term (see Appendix B for details) and $T(\Omega)$ is of the form:

$$T(\Omega) = \lambda_r T_r + \lambda_\mu T_\mu, \quad (11)$$

with:

$$T_r = \int_0^1 \int_0^{R_\odot} f_r(r, \mu) \left(\frac{\partial^i \Omega(r, \mu)}{\partial r^i} \right)^2 dr d\mu, \quad (12)$$

$$T_\mu = \int_0^1 \int_0^{R_\odot} f_\mu(r, \mu) \left(\frac{\partial^j \Omega(r, \mu)}{\partial \mu^j} \right)^2 dr d\mu. \quad (13)$$

This can be regarded as a measure of smoothness of the rotation $\Omega(r, \mu)$. The functions f_r and f_μ are used to assign different weights to the smoothing terms for different positions r and μ . It should be noticed, however, that well chosen functions together with first derivatives ($i = j = 1$) can lead to the definition of flatness given by Sekii (1991): $T(\Omega) = \iint \|\nabla \Omega\|^2 r dr d\theta$. The choice of the so-called trade-off parameters λ_r and λ_μ depends on the data from which we perform the inversion and is discussed in the next section.

Finally, let us define the χ^2 which characterizes how the observed splittings are approached by the solution $\bar{\Omega}(r, \mu)$:

$$\chi^2 = \sum_{nlm} \left(\frac{\Delta \nu_{nlm} - \iint K_{nlm}(r, \mu) \bar{\Omega}(r, \mu) dr d\mu}{\sigma_{nlm}} \right)^2. \quad (14)$$

This value corresponds to the first term in the sum that defines $J(\Omega)$ Eq. (B2).

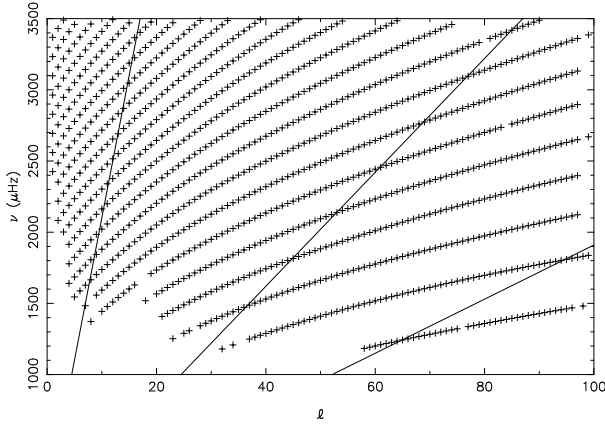


Fig. 1. $l - \nu$ diagram showing the modes included in the LOWL 2 year dataset. Solid lines indicate the values of ν/L that correspond to modes with turning points $r_t=0.4, 0.85, 0.95R_\odot$ from the left to the right.

4. Data and inversion parameters used

4.1. The data: LOWL observations

The LOWL instrument is a Doppler imager based on a Potassium Magneto-Optical Filter that has been operating on Mauna Loa, Hawaii since 1994 (see Tomczyk et al. (1995a) for a detailed description). Both low- and intermediate-degree p-modes can be observed with this instrument.

The modes used in this paper are shown in Fig. 2. The estimations of frequency splittings result from a two year period of observation (2/26/94 - 2/25/96). The first year of observation has been analyzed and inverted by Tomczyk et al. (1996) and is referred as the one year dataset in the following. The second year of observations has been analyzed separately and an unweighted average of the two resulting datasets has been performed to produce the data that we use in this work. These data contain 1102 modes (n, l) with degrees up to $l = 99$ and frequencies lower than $\nu = 3500 \mu\text{Hz}$. For each mode, individual splittings are given by, at best, five a-coefficients of their expansion on orthogonal polynomials $Q_j^l(m)$ defined by Schou et al. (1994):

$$\Delta\nu_{nlm} = \sum_{j=1}^{N_j^l} a_j^{nl} Q_j^l(m) \quad \begin{cases} N_j^l = 2l & l = 1, 2 \\ N_j^l = 5 & l \geq 3 \end{cases} \quad (15)$$

Estimations of standard deviations are given for each of these a-coefficients. To first order, the solar rotation contributes only odd j a-coefficients to the expansion Eq. (15). Even indexed a-coefficients arise from aspherical perturbations, centrifugal distortion and magnetic fields.

We have inverted both odd indexed a-coefficients and the set of splittings reconstructed from these coefficients. The errors assigned to these splittings are discussed in Appendix B. A χ^2 value can be calculated from the inversion of the a-coefficients by the first term in the sum Eq. (B7).

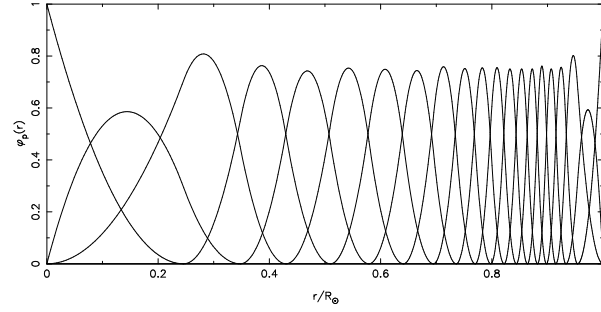


Fig. 2. Basis of $n_r = 21$ B-splines functions of order 3 with a distribution of break points calculated from the density of turning points relative to the set of modes plotted in Fig. 1

4.2. The choice of inversion parameters

4.2.1. Splines basis

In all inversions shown in this paper the set of all B-splines $\psi_q(\mu)$ with $1 \leq q \leq n_\mu = 10$, forms a basis for the linear space of the set of the piecewise polynomials of order 3 having their first derivatives continuous in $]0, 1[$ and with a distribution of break points, i.e. a partition Δ of $[0, 1]$ (see Appendix A), equidistant in $\mu = \cos(\theta)$. Doing this we obtain a finer discretization near the equator than near the pole, in agreement with the fact that among all of the observed modes only a few of them have significant amplitude near the pole. The choice of only a few basis functions ($n_\mu = 10$) to describe the latitudinal dependence of the rotation rate is related to the low number of odd indexed a-coefficients (3 maximum) given by observers to describe the azimuthal- or m -dependence of each splitting through Eq. (15).

B-splines in radius $\varphi_p(r)$ with $1 \leq p \leq n_r = 21$ will also be piecewise polynomials of order 3 with their first derivatives continuous at each break point, but the partition of $[0, R_\odot]$ is chosen such that the number of basis functions used to describe an interval in radius is proportional to the number of modes having their turning points located in this interval (Fig. 2). Compared with an equally spaced partition with the same number of points, this distribution allows a better resolution in the layers which are well described by the data and acts as a regularization term in less well constrained zones.

4.2.2. The trade-off parameters λ_r and λ_μ

Currently, most inverters who use this kind of regularization in helioseismic inversions take $i = j = 2$ in the regularization terms Eqs. (12) and (13) (Schou et al. 1994). Here the code allows constraining with the first derivative of the rotation in latitude (i.e. $j = 1$). Using a high weight in the core (with a function $f_\mu(r, \mu) \propto 1/r^2$ for example), this constraint is in better agreement with the regularity condition at the center given by Eq. (8). Both cases ($j = 1, 2$) have been performed and are discussed in the following with $f_r = r/R_\odot^2$ and $f_\mu = R_\odot^{2j-1} r^{-2j}$.

A generalization of the so-called L-curves currently used in one dimensional problems (Hansen 1992a, b) can be a guide for

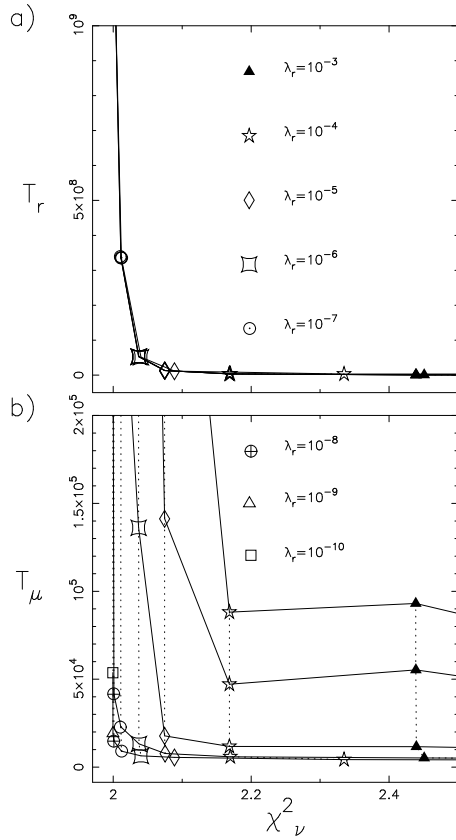


Fig. 3a and b. L-curves obtained by inverting the a-coefficients from the dataset shown in Fig. 2. **a** Regularization term in radius (T_r) (with second derivative ($i = 2$)) and **b** regularization term in latitude (T_μ) (with first derivative ($j = 1$)) against the χ_ν^2 value. Each graph marker corresponds to one value of λ_r . Full curves join points with the same ratio $\alpha = \frac{\lambda_r}{\lambda_\mu}$ ($\alpha = 10^4, 10^2, 1, 10^{-2}, 10^{-4}$ from the top to the bottom) and dotted curves have the same λ_r .

the choice of the trade-off parameters λ_r and λ_μ . The aim is to find parameters that minimize both the χ^2 value obtained for the fit of data and the two regularization terms T_r and T_μ . In the limit of strong regularization (large λ_r and λ_μ) which aims to minimize T_r and T_μ , a small decrease in T_r and T_μ can be obtained only at the expense of a rapidly increasing χ_ν^2 value and the solution does not give a good fit of the data anymore. On the other hand, in the limit of low regularization which aims to minimize the χ_ν^2 value, a little better fit of the data can be obtained only at the expense of a strong increase of the terms T_r and T_μ and the solution presents important oscillations. A good choice of trade-off parameters should be near the intersection of these two limit regimes.

Fig. 3 is a plot of the value of each regularization term against the $\chi_\nu^2 = \chi^2/\nu$ value for different choices of λ_r and λ_μ (ν being the number of degrees of freedom of the system i.e. the difference between the total number of a-coefficients N_a and the number $n_\mu(n_r - 1) + 1$ (see Appendix A) of searched coefficients w_{pq}).

An interesting result is that, on Fig. 3a, all the points which are labeled by the same λ_r but different λ_μ have nearly the same location except for values of $\alpha = \frac{\lambda_r}{\lambda_\mu} \leq 10^{-4}$ and $\lambda_r \geq 10^{-4}$. We define the corner of a curve that joins points with the same ratio α (full curves on Fig. 3) as the nearest point of the curve to the intersection of the two limit regimes asymptotes. For $\alpha = 10^{-4}$ the χ_ν^2 value begins to increase rapidly for the largest values of λ_r (the star graph marker goes on the right). For $\alpha < 10^{-4}$ (not shown on the figure) the corners of the L-curves give larger values of T_r and the corresponding values of parameters must be disregarded because they do not lead to the best compromise between the regularization and the fit of the data. Thus it appears that, near the corners of the L-curve, the χ_ν^2 and T_r values do not depend on the value of λ_μ for a large domain of variation of the parameter α ($10^{-4} \leq \alpha \leq 10^4$): they depend only on λ_r . Consequently we minimize both the T_r and χ_ν^2 values by choosing λ_r at the corner of the L-curve i.e. $\lambda_r = 10^{-6}$.

The choice of λ_μ is then given by the analysis of Fig. 3b. On this figure, as α decreases the position of the L-curve becomes lower showing that for a given value of λ_r , the λ_μ value must be as large as possible (keeping in the previous interval for α) if one wants to reduce the value of the regularization term in latitude.

According to these two figures, a choice near $\lambda_r = 10^{-6}$, $\lambda_\mu = 10^{-2}$ tends to minimize both the χ_ν^2 value and the two regularization terms. When the regularization term in latitude T_μ is chosen with second derivative ($j = 2$), the corresponding plots have similar behaviors but the domain of variation of α , for which χ^2 and T_r depend only on λ_r , is smaller ($10^{-3} \leq \alpha \leq 10^4$). In this case the optimal choice for trade-off parameters becomes $\lambda_r = 10^{-6}$, $\lambda_\mu = 10^{-3}$. The inversion of individual splittings, instead of a-coefficients, leads to the same results for the choice of trade-off parameters and the L-curves analysis is not sensitive to the surface constraints parameter λ_s .

L-curves are a useful tool to study variations and mutual dependencies of each term in Eq. (10) for different choices of trade-off parameters and functions f_r and f_μ . Nevertheless other criteria for the optimal choice of trade-off parameters are possible (Craig & Brown 1986; Thompson & Craig 1992). In particular, for the solar rotation problem, the method of generalized cross validation (GCV) (Golub & Van Loan 1989) has been applied to the 1D RLS inversion method by Thompson (1992) and Barrett (1993). For a local estimation of the quality of the solution, we must look at the balance between the effect of propagating input errors and the resolution (as defined in Appendix C) reached at a target location (r_0, μ_0) . Thus a local optimal choice of trade-off parameters could be based on plots showing resolution against the error on the inferred rotation rate for different choices of trade-off parameters. Such curves have been plotted by Christensen-Dalsgaard et al. (1990) for different 1D inversion techniques and by Schou et al. (1994) for a 2D inversion.

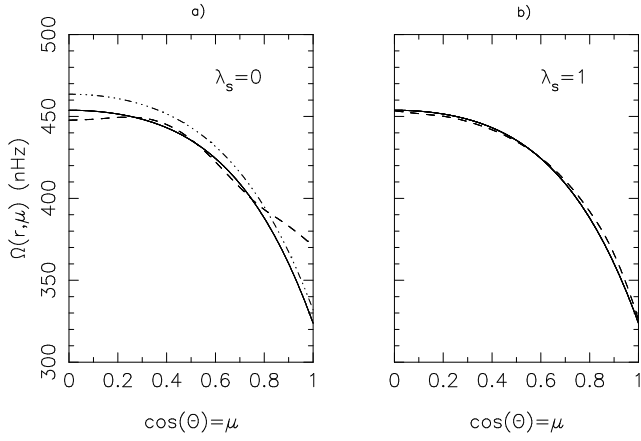


Fig. 4a and b. Inferred surface rotation rates against latitude from inverting a-coefficients. The solid curves show the observations of the plasma surface rotation Eq. (6). The dot-dashed curve shows the observations of the small magnetic feature surface rotation Eq. (7). The dashed curves show the inferred rotation rates: **a** inversion without surface constraint, **b** inversion with plasma surface constraints and $\lambda_s = 1$ (This solution is the same as the one shown in Fig. 7).

4.2.3. Surface constraints and the λ_s parameter

Different surface constraints can be used and introduced in Eq. (B2) with the parameter λ_s which defines the weight assigned to the fit of surface observations. The choice of surface constraints is suggested by the behavior of $\Omega(R_\odot, \mu)$ obtained if we do not impose any surface constraint ($\lambda_s = 0$) and with the previous choice of trade-off parameters (Fig. 4a).

This figure clearly points out that the surface rotation estimated from the helioseismic data alone is closer to the plasma observations than to the small magnetic feature observations. However, the estimated surface rotation has no latitudinal dependence in the region covering 30° around the equator which is in evident contradiction with all surface observations and can be a consequence of the lack of high degree modes in the data. Thus we have to fix the value of λ_s in such a way that the rotation rate obtained at the surface becomes close to the imposed surface values $\Omega_s(i)$ at the $n_\mu = 10$ points.

Let us define the χ_{surface}^2 value by:

$$\chi_{\text{surface}}^2 = \frac{1}{n_\mu} \sum_{i=1}^{n_\mu} \left(\frac{\Omega_s(i) - \Omega(R_\odot, \mu_i)}{\sigma_i} \right)^2, \quad (16)$$

and the relative contribution $p(\lambda_s, r_0, \mu_0)$ of the surface term to the estimated rotation rate at (r_0, μ_0) by (according to Eq. (C1)):

$$p(\lambda_s, r_0, \mu_0) = \frac{100}{\bar{\Omega}(r_0, \mu_0)} \sum_{i=1}^{n_\mu} \tilde{C}_i(r_0, \mu_0) \Omega_p^m(\mu_i), \quad (17)$$

where $\tilde{C}_i(r_0, \mu_0)$ is a function of λ_s .

The Fig. 5a shows the variations against λ_s of the relative contribution of the surface term to the estimated rotation rate at the solar surface ($r_0 = R_\odot$) and at the equator ($\mu_0 = 0$).

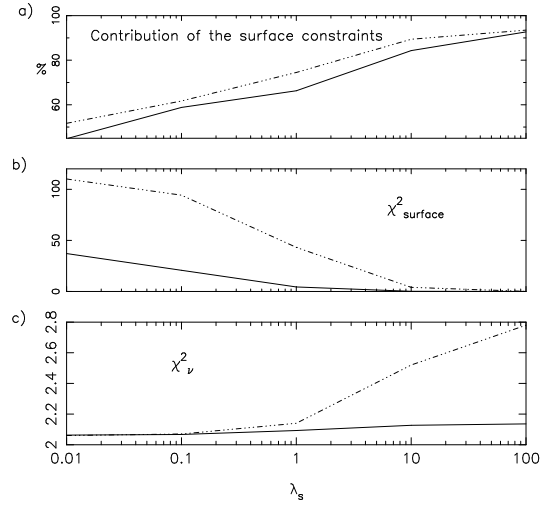


Fig. 5a–c. Variation of, **a** the relative contribution of the surface term in the estimation of the rotation rate at the surface and the equator (i.e. $p(\lambda_s, R_\odot, 0)$) Eq. (17), **b** the χ_{surface}^2 value and **c** the χ_ν^2 value, against λ_s and by inverting a-coefficients. Dot-dashed curves are for the small magnetic feature observations and full curves for the plasma observations used as surface constraints.

The Fig. 5b and c show the variations of χ_{surface}^2 and χ_ν^2 against λ_s for the two kinds of observations Eq. (6) and Eq. (7) used as surface constraints. With the use of plasma rotation observations, we can obtain a small χ_{surface}^2 value for $\lambda_s = 1$ and the helioseismic data still contributes more than 30 percent in the computation of the surface rotation rate. If we want to obtain roughly the same value of the χ_{surface}^2 with the use of the small magnetic feature observations, we have to set $\lambda_s = 10$ and then the helioseismic data contributes less than 10 percent in the computation of the surface rotation rate.

Furthermore, as χ_{surface}^2 decreases, the χ_ν^2 value increases greatly for the small magnetic feature constraint (from 2.0 for $\lambda_s = 0$ up to 2.5 for $\lambda_s = 10$) but not so much for the plasma constraints (Fig. 5b, 5c). This behavior and the very large value of χ_{surface}^2 in Fig. 5b for small magnetic feature clearly indicates that the use of these observations for surface constraints is not compatible with helioseismic data, probably because these observations correspond to the rotation not of the solar surface but of deeper layers.

The Fig. 6 shows the variation of the surface contribution with depth (at fixed $\lambda_s = 1$ and at the equator), showing that the major contribution of the surface constraints occurs above $0.98R_\odot$. Nevertheless some residual (negative) contributions exist below this depth and are more important for the small magnetic feature observations than for the plasma observations.

For these reasons we choose in the following to use plasma observations as surface constraints with $\lambda_s = 1$. With this choice, the inferred rotation rate, shown in Fig. 4b as a function of latitude at the surface, is close to the observed one and remains compatible with LOWL data (Fig. 5c).

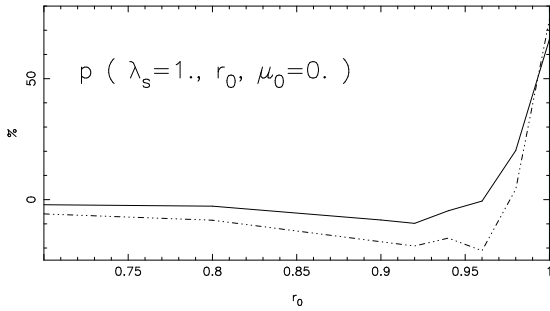


Fig. 6. Variation with depth of the relative contribution of the surface term in the estimation of the rotation rate at the equator and for $\lambda_s = 1$. The line styles are the same as in Fig. 5a-c.

5. Results and discussions

The 2D solar rotation rate obtained by inverting the a-coefficients of LOWL data and the corresponding averaging kernels are given respectively in Figs. 7 and 9. In order to see what could hypothetically be achieved with individual splittings, we made the (unjustified) assumption that the higher a-coefficients are all identically zero and built the corresponding individual splittings. The inversion of these splittings and the corresponding averaging kernels are given respectively in Figs. 8 and 10. The averaging kernels are presented in Appendix C and can be used to assess the quality of the solution and the resolution that we can obtain at different target locations.

5.1. About the χ^2 value

Let us discuss first, the χ^2_ν values obtained at the corner of L-curves. This value is not enough to quantify the quality of the solution but can reveal some problems in the analysis or in the data themselves. The inversion of a-coefficients with $\lambda_s = 0$ leads to a value around $\chi^2_\nu = 2.0$. The value of 2.0 for this parameter is highly improbable for a system with many degrees of freedom and reveals that we can not produce a rotation profile by our RLS inversion that agrees strictly with the LOWL data. We note however that this value was higher (around 2.5 at the corner of the L-curves) with a data set covering only the first year of observations. With the two years dataset, the inversion of only the modes for which $\nu/L > 40 \mu\text{Hz}$ leads to the same value of $\chi^2_\nu = 2.0$, so that the more superficial p-modes do not appear to be particularly subject to systematic errors which was a concern in an analysis of the first 3 months of LOWL data (Tomczyk et al. 1995b).

We remark that the χ^2/N value obtained by inverting individual splittings with weights (or errors) specified as explained in Appendix B (where N is the difference between the number of splittings and the number of searched coefficients), is around $\chi^2/N = 0.13$. Nevertheless, this value is not significant because although the hypothesis of independence of individual splittings is useful to compute their weights in the minimization process (see Appendix B, Eq. (15) implies that individual splittings are dependent, so that the real number of degrees of freedom is still

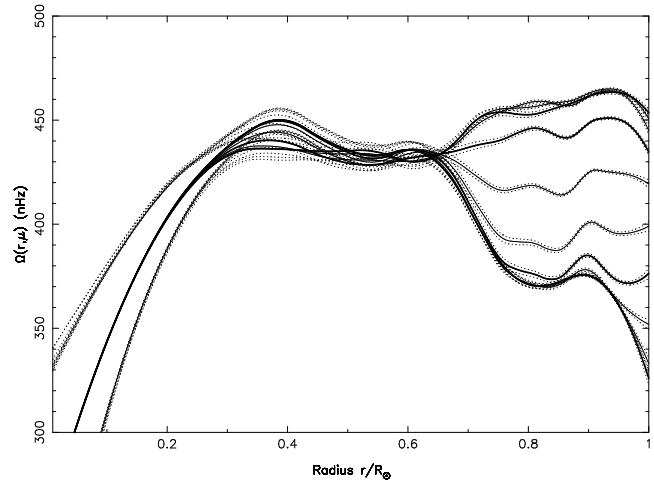


Fig. 7. Inferred rotation rate obtained by inverting a-coefficients, plotted against the solar radius for ten latitudes from the equator up to the pole. Bold curves correspond to colatitudes $\theta = 90, 60, 30, 0^\circ$ from the top to the bottom. Dotted curves are the corresponding 1σ errors.

given from the number of a-coefficients (assumed to be independent) even when individual splittings are inverted. Since, the total number of splittings is on average about 15 times higher than the number of odd indexed a-coefficients, the resulting χ^2_ν value is still around $0.13 \times 15 \simeq 2.0$. We note however that this discussion is valid only on average because the actual ratio between the number of individual splittings and a-coefficients is obviously l -dependent leading to a radial gradient in the apparent improvement on the errors.

The input errors of the a-coefficients are derived from the formal errors when fitting the power spectra and are known to underestimate the true errors. This is the most likely cause for the large values of the χ^2_ν . Additionally, systematic errors in the data could contribute to the value of the χ^2_ν . Also, our results are obtained under the assumption that the hypothesis made in Sect. 2, and the integral expression Eq. (2) for the splittings, are valid for all observed modes. Overly constraining the hypothesis in the forward analysis, as well as some unknown bugs in the inversion process, may also increase the value of χ^2_ν .

5.2. Inversion of a-coefficients

Fig. 7 shows the variations of the inferred rotation rates against the solar radius from the inversion of a-coefficients. The different inversion parameters have been chosen as discussed in the previous sections with, in particular, $\lambda_s = 1$ for the plasma surface constraints. The solution shown in this figure is in good agreement with the result obtained at $\theta = 30, 60, 90^\circ$ between 0.2 and 0.85 solar radius by Tomczyk et al. (1995b) who have inverted a-coefficients from the first three months of LOWL data. The rotation rate presents no variation with latitude at $0.2R_\odot$ with a value around 410 nHz and a transition, between 0.65 and $0.75R_\odot$, to a latitudinal dependent rotation that leads to rotation rates around 370 nHz at 30° of colatitude, 410 nHz at mid-latitude and 460 nHz at the equator for depths between

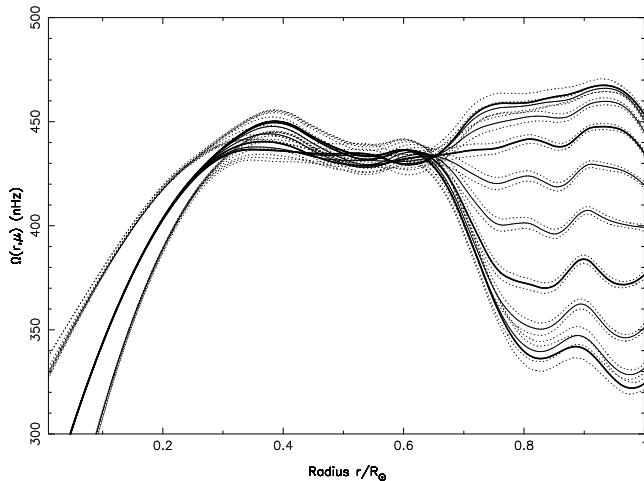


Fig. 8. The same as Fig. 7 but using individual splittings

0.75 and $0.85R_{\odot}$. By inverting the a-coefficients, the inferred rotation has no significant latitudinal variation between 0.75 and $0.95R_{\odot}$ in zones covering 20° around the pole and 20° around the equator.

In the radiative interior, between 0.45 and $0.65R_{\odot}$ we find no significant variation of the rotation rate with radius and latitude. Tomczyk et al. (1995b) found a local maximum at $0.4R_{\odot}$ occurring for all latitudes. This latitudinal independence was due to the fact that at these radii the kernels for all latitudes were all centered at the equator and very similar. In our results with two years of data, the rotation rate for colatitudes from the equator to 60° is found constant for radii between 0.3 to $0.7R_{\odot}$ at a value of 430 nHz. Around $r = 0.4R_{\odot}$ we find a small latitudinal dependence with a maximum at the pole. This difference with previous work may be due to a better latitudinal localization of the averaging kernels obtained at this depth with the two year dataset (kernels at $r_0 = 0.4R_{\odot}$, $\theta_0 = 90^{\circ}$ and $r_0 = 0.4R_{\odot}$, $\theta_0 = 45^{\circ}$ are clearly distinguishable (Fig. 9)). However, this small latitudinal dependence remains marginally significant if we take into account the errors found on the solution at this depth (σ over 5 nHz at the equator and at the pole).

5.3. Inversion of individual splittings

Fig. 8 shows the inferred rotation rate deduced from the inversion of individual splittings. Doing so is equivalent to assuming that the higher (unmeasured) a-coefficients are zero. The rotation rate is very close to that of Fig. 7 except in the convection zone near the equator and the pole. These differences may be analyzed by looking at the averaging kernels.

The kernels obtained by inverting individual splittings (Fig. 10) indicate that we can obtain a better latitudinal resolution than by inverting a-coefficients (Fig. 9) for targets located at radii larger than $0.5R_{\odot}$. In fact, by using a-coefficients directly, the number of these coefficients (i.e. 3) seems to set a limit to the latitudinal resolution around $\Delta\theta = 90^{\circ}/3 = 30^{\circ}$ ($\Delta\theta \simeq 29^{\circ}$ is the best latitudinal resolution reached in Fig. 9). This result

is not surprising since, in a first approximation, the a_1 coefficients correspond to rotation constant on spheres and higher order coefficients specify the deviation from this solid rotation, then their number is strongly related to the latitudinal resolution that we can expect. Obviously, the better latitudinal resolution reached in individual splittings inversion induces higher 1σ errors on the solutions (e.g. $\sigma = 2.98$ nHz at $r_0 = 0.9R_{\odot}$ at the equator in Fig. 10 against $\sigma = 0.72$ nHz for the same location in Fig. 9) so that the rotation obtained near the equator remains compatible, at the 1σ level, with that given by the inversion of a-coefficients. Nevertheless, this is not the case near the pole where the difference in the rotation rates is over 3σ . In this zone we must look not only at the resolution but also at the localization of averaging kernels. By inverting a-coefficients, averaging kernels calculated at the pole remain localized at best at 30° of colatitude for all depths (see θ for the four lower panels in Fig. 9) although, by inverting individual splittings, we can obtain a peak with a maximum value separated only by 15° from the pole at $0.9R_{\odot}$. These remarks could be enough to explain the differences in rotation rates obtained near the pole in the convection zone and seems to argue in favor of the use of the inversion of individual splittings to probe these zones since the inversion of a-coefficients does not allow us to constrain latitudes higher than 60° . Nevertheless, we must keep in mind that the rotation obtained near the pole is related to the real rotation rate only under the assumption that the a_j coefficients are null for $j > 3$. These coefficients are certainly small but not null, therefore this result will change when more accurate data will become available.

Thus, when using a-coefficients inversion, the regularization forces flatness in latitude when there are no data and the resolution is poor. On the other hand, when using individual splittings, we are forcing the behavior of the rotation near the pole leading to an apparent, but not real, increase in the resolution. This result is however interesting from the point of view of exploring what one might get in terms of averaging kernel and latitudinal resolution if one had more a-coefficients or even individual splittings.

5.4. The rotation of surface layers

The rotation of layers just beneath the solar surface, and in the convection zone is of great importance for our understanding of the solar dynamo and its observed consequences. Some radial gradient of the solar rotation has been suspected in order to explain the different rotation rates, deduced from the observations of various surface indicators, as a consequence of the different depths where these tracers are anchored (e.g. Snodgrass & Ulrich 1990). Therefore it is of interest to look at the rotation rate calculated in this zone by inverting helioseismic data. In the two year dataset, modes with $\nu/L < 40$ μ Hz are no longer thought to be subject to systematic errors and according to Figs. 2 and 2 we believe that the number of superficial p-modes are now enough to try to describe the rotation between 0.85 and 0.95 solar radii.

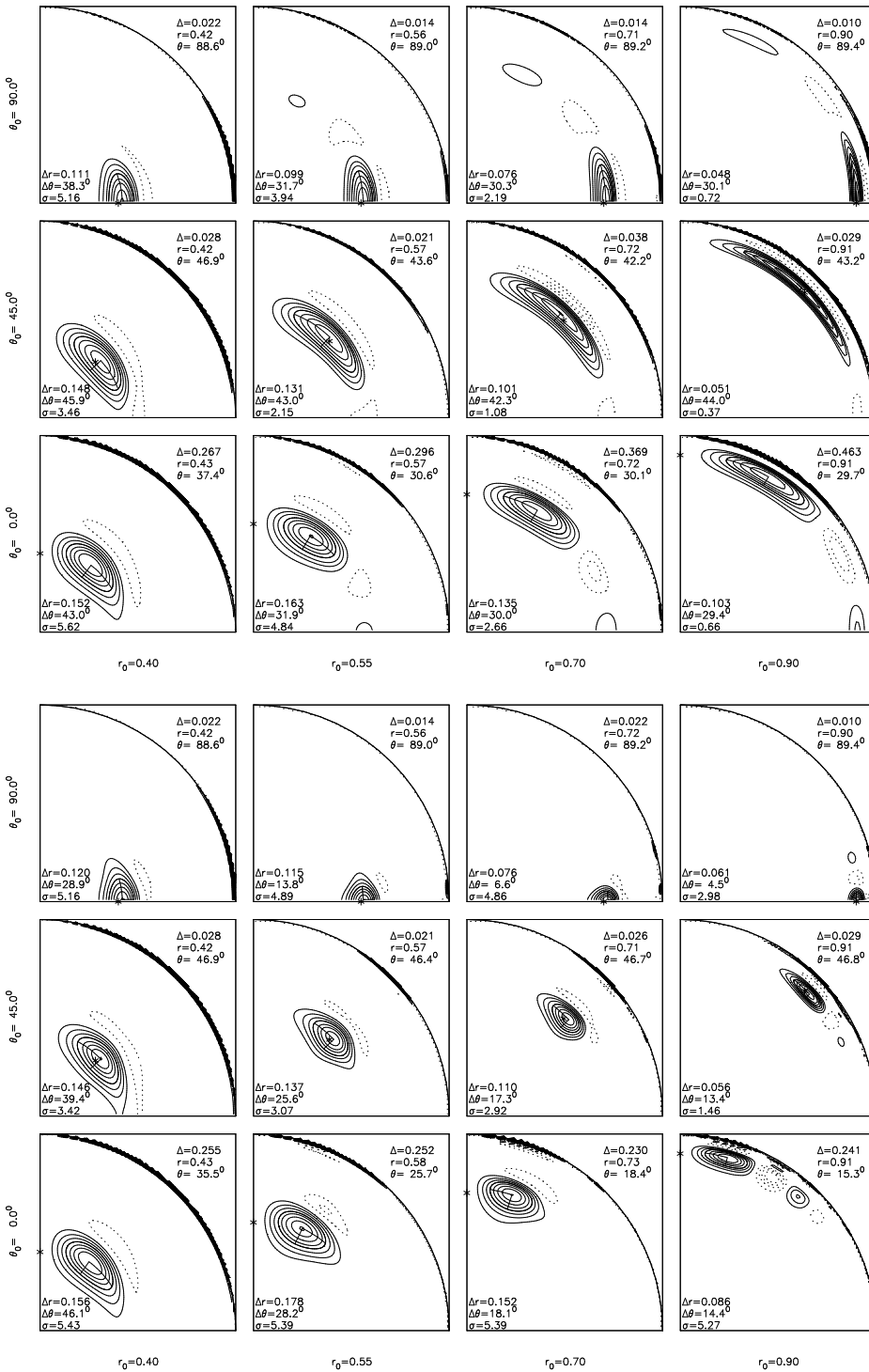


Fig. 9. Averaging kernels corresponding to the inversion of a-coefficients (Fig. 7). For each panel, the contour spacing is defined by the value of the averaging kernel at (r, θ) divided by eight. Positive contours are shown solid, and negative contours dotted. For clarity the zero contour have been omitted. Δ is the geometrical distance between the position (r, θ) of the maximum value of the peak and the point (r_0, θ_0) shown by a star. Δr and $\Delta \theta$ denote the radial and latitudinal resolution as defined in Appendix C. σ is the 1σ error (in nHz) calculated at (r_0, θ_0) and shown by dotted lines on Fig. 7.

Fig. 10. Averaging kernels corresponding to the inversion of individual splittings (Fig. 8) (See caption Fig. 9).

The introduction of the surface constraints does not modify the solution below $0.95R_\odot$. Above this depth, the contribution of surface constraints increases and represents more than 70 percent in the calculation of the inferred rotation rate at the surface (Fig. 6).

In Figs. 7 and 8 the solution reaches a maximum at $0.9R_\odot$ between the pole and 30° of latitude. The radial and latitudinal resolution obtained at $0.9R_\odot$ ($\Delta r \simeq 0.06R_\odot$, $\Delta \theta \simeq 13^\circ$ at

$\theta_0 = 45^\circ$ in Fig. 10) indicates that the positive gradient between 0.85 and $0.90R_\odot$ may be real in zones between 30° and 60° of latitudes.

The discussion in Sect. 4.2.3 has shown that the LOWL data are more compatible with the plasma observations than with the small magnetic feature observations. Fig. 7 shows that the inferred rotation rate at $0.95R_\odot$ is close to the small magnetic features rate Ω_m ($\Omega \simeq 464$ nHz at the equator). Therefore our

inversion should argue in favor of this depth for the location where small magnetic features are anchored. Nevertheless, this result is different from the one obtained by Thompson et al. (1996) with Global Oscillation Network Group (GONG) data in which the inferred rotation rate at the surface (without setting surface constraints) is close to the rate deduced from the observation of small magnetic features and reaches a maximum near $0.95R_{\odot}$ with a value $\Omega \simeq 470$ nHz at the equator which can correspond to the value observed by Snodgrass & Ulrich (1990) for the rotation of supergranular network. From the inversion of LOWL data, this value is never reached but the observation of modes with higher degrees is certainly necessary for making a more reliable inference about the rotation of these layers.

Finally, we note that Antia et al. (1996), who have investigated the Sun's rotation rate in the equatorial plane by inverting BBSO datasets for the years 1986, 1988, 1989 and 1990, have found a locally enhanced rotation rate near $0.9R_{\odot}$. They have pointed out that this behavior shows variation with time. Our solution covering years 1994 to 1996 does not show a bump with significant amplitude near $0.9R_{\odot}$ in the equatorial plane.

5.5. The solar tachocline

At the base of the convection zone, from 0.75 down to 0.65 solar radii, the rotation rate makes a transition to a latitudinally independent behavior which persists in the whole radiative interior. This transition layer is sometimes called the solar tachocline and the evaluation of its thickness which can be related to the horizontal behavior of the turbulent viscosity is of primary importance for our understanding of the eddy diffusivity (Spiegel & Zahn 1992). If we assume that this transition occurs at all latitudes with roughly the same thickness, we can use in this zone the results obtained by inverting a-coefficients that provide worse latitudinal resolution but better radial resolution than the inversion of individual splittings. Unfortunately, the radial resolution reached in the transition zone ($\Delta r \simeq 0.08R_{\odot}$ at the equator down to $\Delta r \simeq 0.14R_{\odot}$ at the pole in Fig. 9) does not allow us to specify how sharp this transition is. It is not more than 0.1 solar radius but it could be less. Thus in our analysis, the solar tachocline remains unresolved, even with a two year dataset. The radial resolution reached at $0.7R_{\odot}$ with the one year dataset was slightly poorer (namely $\Delta r \simeq 0.083R_{\odot}$ compared to $\Delta r \simeq 0.076R_{\odot}$ at the equator). This small increase in the radial resolution could be due to the lower errors of the 2 year dataset but we think that we are approaching the fundamental limit of resolution at least at the base of the convection zone with this dataset. Further improvement will be very difficult and we may need to resort to non-linear inversion methods. For this work, continuing the ground-based observations in addition to the space missions would be very important if the width and position of the solar tachocline does not vary too much during the solar cycle.

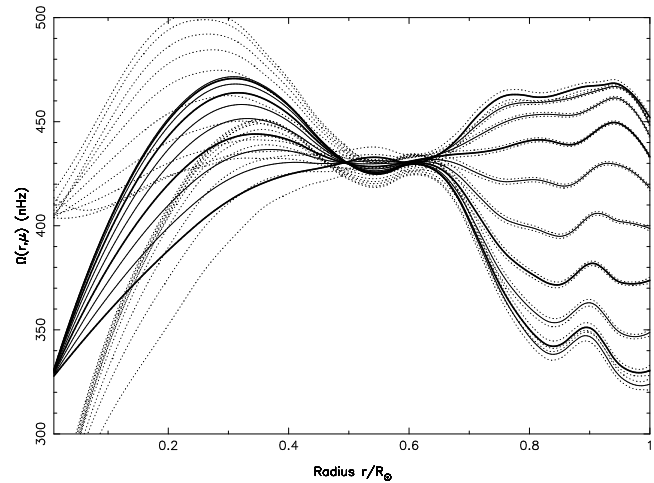


Fig. 11. Inferred rotation rate obtained by inverting individual splittings with $j = 2$ in the regularization term T_{μ} Eq. (13), $\lambda_r = 10^{-6}$, $\lambda_{\mu} = 10^{-3}$.

5.6. The rotation of the core

Below $0.4R_{\odot}$ our solution is compatible with a core that rotates slower than the radiative interior and gives $\Omega_0 = 260 \pm 80$ nHz for the value in the center. As already discussed in Tomczyk et al. (1996), this low value of Ω_0 is partly due to the low frequency splittings measured for the modes $l = 1$ and that we use in our inversion. Nevertheless, at these depths the averaging kernels are large, not well localized and consist of several peaks, so that the result and the corresponding errors are difficult to interpret. In particular, the latitudinal independence found at these depths results from the choice $j = 1$ in the regularization term T_{μ} Eq. (13).

Fig. 11 shows an instructive example of a solution obtained by setting $j = 2$ and taking the trade-off parameters given by the corner of the L-curves that correspond to this choice (see Sect. 4.2.2). Above $0.4R_{\odot}$ the solution is roughly identical to the solution of Fig. 8. The fact that we insure the regularity of the solution at the center avoids finding several values at $r = 0$ and gives in that case $\Omega_0 = 330 \pm 80$ nHz, but the solution shows a significant latitudinal variation below $0.4R_{\odot}$ contrary to the case with $j = 1$. Therefore the latitudinal dependence is very sensitive to the order of the derivative used in the regularization term and reveals that a reliable description of the latitudinal dependence in this region requires data with lower errors for the low-degree p-modes. Thus we think that the choice $j = 1$ in our code provides an initial way to sound the very deep interior from such global inversions, without searching for a description of a latitudinal dependence in the core that requires very low errors in the data.

6. Conclusion

A two dimensional regularized least-squares inversion code with expansion of the solution in B-splines has been presented.

It includes a condition that insures the regularity of the solution at the center and provides the possibility of adding surface constraints on the rotation rate.

We have inverted the two year LOWL rotational splitting dataset to derive the rotation rate of the solar interior matched to the observed plasma surface rotation rate. Both the inversion of the three a -coefficients and of the individuals splittings reconstructed from these a -coefficients have been performed. The comparison of the results gives an estimation of the improvement of the latitudinal resolution which could be obtained by the knowledge of the individual splittings.

Between 0.4 and $0.85R_{\odot}$, our results are in good agreement with the previous work of Tomczyk et al. (1995b) who have used the first three month dataset. The small maximum at $0.4R_{\odot}$ obtained previously is however smoothed for polar latitudes and disappears for equatorial rotation.

The 2 year dataset allows a description of the internal rotation rate with depth and latitude from 0.4 up to 0.95 solar radii with increasing radial resolution. At the base of the convection zone, the width of the transition zone is found to be smaller than 0.1 solar radii, in agreement with Thompson et al. (1996). We have shown that the LOWL data are compatible with the surface rotation estimated by plasma observations and confirm an increase of the rotation below the surface up to values measured by magnetic feature observations for equatorial latitudes.

Our solution is compatible with a solar core that rotates slower than the radiative interior. However, improved observations are needed to sound the region below $0.4R_{\odot}$ more accurately and with latitudinal resolution. In addition to the ground based networks, the instruments aboard the SOHO satellite will hopefully provide these observations in the near future and add the possibility of detecting low frequency p-modes as well as g-modes which have their maximum amplitude in the solar core.

Acknowledgements. The numerical computations have been performed on the Cray C98 (IDRIS, CNRS, Orsay). We acknowledge financial support from the GDR 131 from CNRS. S. Tomczyk acknowledges support from the US National Science Foundation through base funding of HAO/NCAR. We wish to thank the anonymous referee for his constructive remarks.

Appendix A: the space of solutions

In this work, we search the rotation rate as a piecewise polynomial of arbitrary order in two dimensions. Let us define more precisely what piecewise polynomials are: a piecewise polynomial $\mathcal{P}(q)$ of order m on a given partition Δ of $[q_1, q_n]$ $\Delta \equiv [q_1 < q_2 < \dots < q_{n-1} < q_n]$ is defined as a function which coincides, on each sub-interval $[q_i, q_{i+1}]$ $1 \leq i < n$ with a polynomial of degree $m - 1$. We can define at each break point the kind of connection which is required between the right and the left pieces of polynomials. Formally, the rules of connection can differ from one break point to the next: at some of them, $\mathcal{P}(q_i)$ can be discontinuous, at some others the left and right pieces can be tied to fulfilling the continuity of their first derivatives or only of $\mathcal{P}(q_i)$, ...etc.

It can be shown that a basis of such a space of piecewise polynomials can be obtained from B-splines in 1 dimension and a tensorial product of B-splines in two dimensions (Schumaker 1981). B-splines basis are a local basis. Moreover, at a given q ($q \in [q_1, q_n]$), only m B-splines of order m are not identically zero and their sum is equal to 1. These properties have two principal useful consequences in our case. First they are easy to compute and the evaluation of the rotation at a given target location needs only a few calculations. Second, they allow us to easily study the boundary conditions in the core and at the solar surface.

Using $\varphi_p(0) = \delta_{p,1}$ and $\varphi_p(R_{\odot}) = \delta_{p,n_r}$ we obtain respectively at the surface and the center:

$$\Omega(R_{\odot}, \mu) = \sum_{q=1}^{n_{\mu}} \omega_{n_r, q} \psi_q(\mu), \quad (\text{A1})$$

$$\lim_{r \rightarrow 0} \frac{\partial \Omega(r, \mu)}{\partial \theta} = 0 \Leftrightarrow \omega_{1q} = \Omega_0 = \Omega(0, \mu) \forall q \forall \mu. \quad (\text{A2})$$

From Eq. (A1), the knowledge of the surface rotation at n_{μ} different and well chosen latitudes allows us to fix in theory the n_{μ} coefficients $\omega_{n_r, q}$, ($q = 1..n_{\mu}$) which form a vector named Ω_2 in the following. Nevertheless, the observations of the surface motions Eq. (6) are given with some error bars. Moreover, the depth which defines the solar surface depends on the choice of indicator and may differ from the surface of the solar model which gives the upper boundary for the p-modes. Consequently, we prefer to include these observations in the minimization procedure rather than to calculate directly the vector Ω_2 only from data concerning the motion of the surface.

The relation Eq. (A2) allows us to search less coefficients to describe the core than for the rest of the solar interior. This is reasonable because of the lack of observed modes able to describe this zone even if we invert data including both low and intermediate degrees. This introduces a scalar value Ω_0 which is the value of the rotation at the center of the Sun and that is used only to describe the rotation rate in depth where the first B-spline $\varphi_1(r)$ is not identically zero i.e. in most practical cases under 0.2 solar radii (see Sect. 4.1, Fig. 2)

The relation Eq. (9) becomes:

$$\begin{aligned} \Omega(r, \mu) = & \Omega_0 \varphi_1(r) + \varphi_{n_r}(r) \sum_{q=1}^{n_{\mu}} \omega_{n_r, q} \psi_q(\mu) \\ & + \sum_{p=2}^{n_r-1} \sum_{q=1}^{n_{\mu}} \omega_{pq} \varphi_p(r) \psi_q(\mu). \end{aligned} \quad (\text{A3})$$

Appendix B: the functions $J(\Omega)$

We apply a least-squares method on values of both observed splittings and observed surface rotation. More precisely, we search the vector

$$\Omega = \begin{bmatrix} \Omega_1 \\ \dots \\ \Omega_2 \\ \dots \\ \Omega_0 \end{bmatrix} \text{ where: } \begin{cases} \Omega_1 \equiv (\omega_{pq})_{\substack{p=2..n_r-1 \\ q=1..n_\mu}} \\ \Omega_2 \equiv (\omega_{n_r,q})_{q=1..n_\mu} \end{cases} \quad (\text{B1})$$

by minimizing the quantity:

$$J^{(w)}(\Omega) = \|P^{(w)}(\mathbf{W} - \mathbf{R}\Omega)\|^2 + \lambda_s \|P_s(\Omega_s - \mathbf{L}\Omega_2)\|^2, \quad (\text{B2})$$

where:

- $P^{(w)}$, P_s are the diagonal matrix of the inverse of errors given on splittings and surface rotation values. These errors are therefore used as weights in the whole minimization procedure.
- \mathbf{W} is the vector of observed splittings $\Delta\nu_{nlm}$,
- \mathbf{R} is a matrix computed by the discretization of Eq. (2) using Eq. (A3) and Gaussian integrations.
- Ω_s is the vector of the values of the surface rotation $\Omega_s \equiv (\Omega(R_\odot, \mu_i))_{i=1..n_\mu}$ according to Eq. (6),
- \mathbf{L} is a matrix defined by: $L \equiv (L_{iq})_{\substack{i=1..n_\mu \\ q=1..n_\mu}} L_{iq} = \psi_q(\mu_i)$ according to Eq. (A1) and
- λ_s is a parameter used to define the weight assigned to the fit of surface observations. If $\tilde{\Omega}(\lambda_s)$ is the solution of the problem:

$$\min_{\Omega} J^{(w)}(\Omega), \quad (\text{B3})$$

and $\tilde{\Omega}$ the solution of the equality constrained least-squares problem:

$$\min_{L\Omega_2=\Omega_s} \|P^{(w)}(\mathbf{W} - \mathbf{R}\Omega)\|^2, \quad (\text{B4})$$

then $\lim_{\lambda_s \rightarrow \infty} \tilde{\Omega}(\lambda_s) = \tilde{\Omega}$ (Golub & Van Loan 1989). Therefore a high value of the parameter λ_s tends to give a good fit of these observations but one can take small values or even $\lambda_s = 0$ if the observed p-modes are thought to be adequate to describe the surface rotation.

Unfortunately, up to now most of the observers do not give individual splittings $\Delta\nu_{nlm}$ but rather few coefficients (typically $N_j^l = 5$ or 9) of their expansion on chosen polynomials $Q_j^l(m)$ (Eq. (15)). This latter equation can be rewritten in matrix form:

$$\mathbf{W} = \mathbf{Q}\mathbf{A}, \quad (\text{B5})$$

by building the vector \mathbf{A} of odd indexed a-coefficients for all modes (n, l) and the appropriate rectangular matrix \mathbf{Q} of polynomials $Q_i(m)$ ($i = 1, 3, 5$). Therefore, there are two ways for performing the inversion: we can build all individual splittings from Eq. (B5) and minimize $J^{(w)}(\Omega)$; or we can express a-coefficients as a linear combination of individual splittings:

$$\mathbf{A} = \mathbf{Q}^\dagger \mathbf{W}, \quad (\text{B6})$$

where \mathbf{Q}^\dagger is the pseudo-inverse of \mathbf{Q} (assuming that this one exists for the chosen polynomials), and minimize:

$$J^{(a)}(\Omega) = \|P^{(a)}(\mathbf{A} - \mathbf{R}^{(a)}\Omega)\|^2 + \lambda_s \|P_s(\Omega_s - \mathbf{L}\Omega_2)\|^2, \quad (\text{B7})$$

$$\text{where: } \mathbf{R}^{(a)} = \mathbf{Q}^\dagger \mathbf{R}. \quad (\text{B8})$$

In this case we can use directly the quoted errors on the a-coefficients (matrix $P^{(a)}$).

When we invert splittings, we must take care of weights that we assign to individual splittings through matrix $P^{(w)}$: Eq. (15) implies that individual splittings calculated from a-coefficients are correlated and thus there is no evident diagonal matrix $P^{(w)}$. One possibility is to calculate the true covariance matrix $B^{(w)}$ on individual splittings using Eq. (B5):

$$B^{(w)} = \mathbf{Q}P^{(a)}\mathbf{Q}^\top, \quad (\mathbf{Q}^\top \text{ being the transpose of } \mathbf{Q}) \quad (\text{B9})$$

and to take only the diagonal part of this matrix as matrix $(P^{(w)})^{-2}$ (Sekii 1991; Corbard et al. 1995). This leads to individual errors that depend on m . In this work, however, we assume that individual splittings are uncorrelated and independent of m for each (n, l) (Schou et al. 1992) and we calculate their errors such that they lead at best in a least-squares sense to the errors given on the a-coefficients if these ones were calculated by a least-squares fit to individual splittings. By this way, we obtain individual errors that are higher than in the previous case especially for low m .

In order to have a more immediate interpretation of the result found by inverting individual splittings it will be of much interest to have accurate observations for individual splittings along with their associated errors. This is already the case with the ground based GONG experiment and should probably be possible with the SOHO space mission instruments.

In this paper $J(\Omega)$ denote both $J^{(a)}(\Omega)$ and $J^{(w)}(\Omega)$ depending on the kind of inversion we perform.

Appendix C: averaging kernels

For all linear inversion techniques, the inferred rotation rate at a target location (r_0, μ_0) can be expressed as a linear combination of the data. Namely, in our implementation these data are the splittings $\Delta\nu_{nlm}$ and, if $\lambda_s \neq 0$, the observed rotation rates at the surface $\Omega_p^m(\mu_i)$:

$$\begin{aligned} \tilde{\Omega}(r_0, \mu_0) &= \sum_{nlm} C_{nlm}(r_0, \mu_0) \Delta\nu_{nlm} \\ &+ \sum_{i=1}^{n_\mu} \tilde{C}_i(r_0, \mu_0) \Omega_p^m(\mu_i). \end{aligned} \quad (\text{C1})$$

Averaging kernels $\kappa(r_0, \mu_0, r, \mu)$ are defined by:

$$\tilde{\Omega}(r_0, \mu_0) = \int_0^{R_\odot} \int_0^1 \kappa_{nlm}(r_0, \mu_0, r, \mu) \Omega(r, \mu) dr d\mu. \quad (\text{C2})$$

From Eqs. (2) and (C1) we get:

$$\begin{aligned} \kappa_{nlm}(r_0, \mu_0, r, \mu) = & \sum_{nlm} C_{nlm}(r_0, \mu_0) K_{nlm}(r, \mu) \\ & + \sum_{i=1}^{n_\mu} \tilde{C}_i(r_0, \mu_0) \delta(r - R_\odot, \mu - \mu_i). \quad (\text{C3}) \end{aligned}$$

Here $\delta(x, y)$ denote a Dirac distribution in two dimensions. Each surface constraint induces a term proportional to a δ function, localized at the corresponding point of the surface, in the averaging kernel. The same relations exist when a-coefficients are inverted instead of individual splittings.

From Eq. (C2) the value of the inferred rotation rate $\bar{\Omega}(r_0, \mu_0)$ can be regarded as a weighted average of the true rotation rate where the averaging kernel $\kappa(r, \mu, r_0, \mu_0)$ is the weighting function. Ideal averaging kernels would be close to a $\delta(r - r_0, \mu - \mu_0)$ function leading to $\bar{\Omega}(r_0, \mu_0) = \Omega(r_0, \mu_0)$. In practice averaging kernels have a peak near (r_0, μ_0) and we can evaluate the latitudinal and radial full width at mid height (FWMH) of this peak, $\Delta\theta$ and Δr , respectively. These quantities provide a measure of the resolution of the inversion in the sense that it gives a limit for the finest details that the inversion is able to resolve for a given depth and latitude. It should be noted that averaging kernels formally do not depend on the data but only on errors on these data. Nevertheless they depend on the regularization used (high regularization decreases the resolution) and the regularization used itself depends on the set of data that we want to invert. A complete description of averaging kernels and their properties can be found in Christensen-Dalsgaard et al. (1990) and Schou et al. (1994).

References

Antia H.M., Chitre S.M., Thompson M.J., 1996, A&A 308, 656
 Appourchaux T., Toutain T., Telljohann U., 1994, A&A 294, L13
 Barrett R.K., 1993, On the optimal choice of regularization parameter for the inversion of solar oscillation data. In: Brown T.M. (ed) GONG 1992: Seismic Investigation of the Sun and Stars (A.S.P. Conf. Ser. vol. 42), Astr. Soc. of the Pacific, San Francisco, p. 233
 Chaplin W.J., Elsworth Y., Howe R., et al., 1996, MNRAS 280, 849
 Christensen-Dalsgaard J., Berthomieu G., 1991, Theory of Solar Oscillations. In: Cox A.N., Livingstone W.C., Matthews M.S. (eds) Solar Interior and Atmosphere. Univ. of Arizona Press, Tucson, p. 401
 Christensen-Dalsgaard J., Schou J., 1988, Differential rotation in the Solar Interior. In: Domingo V., Rolfe E.J. (eds) Seismology of the Sun and Sun-like Stars (ESA SP-286), ESA Publication Division, Noordwijk, p. 149
 Christensen-Dalsgaard J., Schou J., Thompson M.J., 1990, MNRAS 242, 353
 Corbard T., Berthomieu G., Gonczi G., Provost J., Morel P., 1995, Solar Rotation from 2D Inversion. In: Hoeksema J.T., Domingo V., Fleck B., Battrick B. (eds) Fourth Soho Workshop: Helioseismologie (ESA SP-376 vol. 2). ESA Publication Division, Noordwijk, p. 289
 Craig I.J.D., Brown J.C., 1986, Inverse Problems in Astronomy: A Guide to Inversion Strategies for Remotely Sensed Data. Adam Hilger, Bristol

Cuyper J., 1980, A&A 89, 207
 Duvall T.L. Jr., Dziembowski W.A., Goode P.R., et al., 1984, Nature 310, 22
 Dziembowski W.A., Goode P.R., Libbrecht K.G., 1989, ApJ 337, L53
 Fröhlich C., Romero J., Roth H., et al., 1995, Sol. Phys., 162, 101
 Gabriel A.H., Grec G., Charra J., et al., 1995, Sol. Phys., 162, 61
 Golub G.H., Van Loan C.F., 1989, Matrix Computations (2nd Edition). The Johns Hopkins Univ. Press, Baltimore
 Gough D.O., 1981, MNRAS 196, 731
 Hansen C.J., Cox J.P., Van Horn H.M., 1977, ApJ 217, 151
 Hansen P.C., 1992a, Inverse Problems 8, 849
 Hansen P.C., 1992b, SIAM Review 34, 561
 Komm R.W., Howard R.F., Solar Phys. 143, 19
 Harvey J.W., Hill F., Hubbard R.P., et al., 1996, Science 272, 1284
 Lazrek M., Pantel A., Fossat E., et al., 1996, Sol. Phys., 166, 1
 Pijpers F.P., Thompson M.J., 1996, MNRAS, 279, 498
 Scherrer P.H., Bogart R.S., Bush R.I., et al., 1995, Sol. Phys. 162, 129
 Schou J., 1991, On the 2-dimensional Rotational Inversion Problem. In: Gough D.O., Toomre J. (eds) Lecture Notes in Physics, Vol. 388, Challenges to Theories of the structure of Moderate Mass Stars, Springer-Verlag, Berlin, p. 93
 Schou J., Christensen-Dalsgaard J., Thompson M.J., 1992, ApJ 385, L59
 Schou J., Christensen-Dalsgaard J., Thompson M.J., 1994, ApJ 433, 389
 Schröter E.H., 1985, Sol. phys. 100, 141
 Schumaker L.L., 1981, Spline Functions: Basic Theory, John Wiley and Sons, New York
 Sekii T., 1990, Two-Dimensional Inversion of Rotational Splitting Data. In: Osaki Y., Shibahashi H. (eds) Lecture Notes in Physics, Vol. 367, Progress of Seismologie of the Sun and stars, Springer-Verlag, Berlin, p. 337
 Sekii T., 1991, PASJ 43, 381
 Sekii T., 1993, MNRAS 264, 1018
 Snodgrass H.B., 1984, Solar phys., 94, 13
 Snodgrass H.B., Ulrich R.K., 1990, ApJ 351, 309
 Spiegel E.A., Zahn J.-P., 1992, A&A 265, 106
 Thompson A.M., 1992, A&A 265, 289
 Thompson A.M., Craig I.J.D., 1992, A&A 262, 359
 Thompson M.J., Toomre J., Anderson E.R., et al., 1996, Science 272, 1300
 Tikhonov A.N., Arsenin V.Y., 1977, Solutions of Ill-Posed Problems, Winston, Washington D.C.
 Tomczyk S., Stander K., Card G., Elmore D., Hull H., Cacciani A., 1995a, Solar Phys. 159, 1
 Tomczyk S., Schou J., Thompson M.J., 1995b, ApJ 448, L57
 Tomczyk S., Schou J., Thompson M.J., 1996, Bull. Astr. Soc. India 24, 245
 Unno W., Osaki Y., Ando H., Saio H., Shibahashi H., 1989, Nonradial oscillations of stars (2nd edition). University of Tokyo press, Japan
 Woodard M.F., Libbrecht K.G., 1993, ApJ 402, L77